Transient grating in a ferrofluid under magnetic field: Effect of magnetic interactions on the diffusion coefficient of translation

J.-C. Bacri,[1,*] A. Cebers,[2] A. Bourdon,[1] G. Demouchy,[1] B. M. Heegaard,[1] B. Kashevsky,[3] and R. Perzynski[1]
[1]*Laboratoire d'Acoustique et Optique de la Matière Condensée, Université Pierre et Marie Curie, Tour 13, Boîte 78, 4 place Jussieu, 75252 Paris Cedex 05, France*
[2]*Latvian Academy of Sciences, Institute of Physics, LV-2169, Salaspils, Republic of Latvia*
[3]*Heat and Mass Transfer Institute, Belarus Academy of Sciences, 15 P. Brovka Street, Minsk 220072, Republic of Belarus*
(Received 1 February 1995)

Diffusion processes in a magnetic colloid are studied by a forced Rayleigh scattering technique under an applied static magnetic field. A periodic spatial modulation of the particle concentration (transient grating) is induced in the colloid with three different field geometries, **B** being either parallel or perpendicular to the grating direction. The value of the translational diffusion coefficient of the particles is given by the transient grating relaxation time. It depends on the magnetic field strength and on the field geometry. A theoretical model based on a mean field approximation taking magnetic interactions of particles under a field into account is given which agrees with experimental results.

PACS number(s): 82.70.Dd, 42.65.Es, 75.50.Mm, 66.90.+r

I. INTRODUCTION

A ferrofluid [1–3] is a colloidal suspension of magnetic particles in a carrier solvent. Such magnetic colloids attract more and more interest because of their spectacular patterns under a magnetic field [4–9] and their numerous technical applications [1,3,4], in particular, in the synthesis of more complex media such as magnetic liquid crystals [10–12], magnetic emulsions [13], and magnetic vesicles [14,15]. In a ferrofluid, the rotational diffusion coefficient of particles is easily determined through a measurement of transient magnetic birefringence relaxation [16–20]. Up to now, only dilute magnetic media have been explored by this technique, with volume fractions Φ of particles ranging from 10^{-4} to 10^{-2}. For its part, the translational diffusion coefficient of magnetic particles has been seldom studied [21–23]: the technique of quasielastic light scattering [21] is not suitable for large colloidal concentrations of ferrofluids because of multiple diffusion processes; the technique of spin echo of neutrons is complex, mixing the contribution [24] of the Brownian dynamics of the particles with that of the dynamics of the magnetic moments inside the particles; transient grating experiments [25] can also lead to a determination of the diffusion coefficient. Such a method has been recently described [26] for ferrofluids. A spatial modulation of concentration of magnetic particles is induced inside the suspension which remains stable [27–29] from a colloidal point of view. The relaxation time of the transient grating gives access to cooperative mass diffusion of particles in the solution (gradient diffusion [30]). One of its main characteristics is that it can be measured in high concentration colloids: $\Phi \simeq 10\%$.

If a magnetic field is applied perpendicularly to the transient grating fringes, the spatial inhomogeneities of the magnetic medium induce a magnetic force which enhances particle diffusion. Anyway the diffusion coefficient, which is proportional to the first derivative of the osmotic pressure, is always sensitive to interparticle interactions. In the present paper, we focus on the magnetic interactions between particles under an applied magnetic field. To study this interaction effect, various configurations of magnetic field with respect to the transient grating fringes have been used. In particular, if the field is parallel to the fringes, the dominant effect is that magnetic interactions slow down the particle diffusion.

After a brief description of the experimental setup, our results are given for the three different geometries of the magnetic field. A mean field model is then developed to account for the variations of the measured diffusion coefficient as a function of the magnetic field in the various geometries.

II. EXPERIMENTAL SECTION

The magnetic fluid used here is an aqueous ferrofluid. The suspended nanoparticles are magnetic monodomains of maghemite (γ-Fe_2O_3), synthesized through Massart's method [31]. The colloidal stability of the solution is ensured by a screened electrostatic repulsion between particles: each particle bears a positive superficial density of charges equal to 0.2 C/m^2 and the carrier medium is an aqueous acidic solution of *p*H 2 and low ionic strength. Colloidal stability is checked through two kinds of experiments: small angle x-ray scattering (SAXS) [32] in zero magnetic field (Laboratoire pour l'Utilisation du Rayonnement Electromagnetique, Orsay) and optical diffraction [33] under magnetic field up to 160 kA/m. No intrinsic field-induced or laser-induced agglomeration is observed. The colloidal volume fraction of particles is measured by chemical titration of iron: $\Phi = 10\%$. The

*Also at Université Paris 7, Tour 13, 2 place Jussieu, 75251 Paris Cedex 05, France.

magnetic volume fraction, slightly smaller (9%), is deduced from the saturation value of the magnetization of the solution at $H=800$ kA/m. Characterizations of particle size are performed on a dilute solution ($\Phi_0 \simeq 1\%$) of the same magnetic particles. A measurement of its initial susceptibility χ_0 [34] leads to a magnetic radius value $R_M=6$ nm (by using the bulk magnetization $m_S=4\times10^5$ A/m). The hydrodynamic radius $R_H=15$ nm is deduced from a determination of the rotational diffusion coefficient of the particles by measuring transient magnetic birefringence [20].

Some of the parameters of the interparticle interactions can be evaluated.

The second virial coefficient κ_T^0 of the osmotic pressure $\pi(\Phi)$ in zero magnetic field and at room temperature is derived from $\pi(\Phi)=\pi_0(\Phi)(1+\frac{1}{2}\kappa_T^0\Phi)$, $\pi_0(\Phi)$ being the expression of the osmotic pressure in the low concentration limit. From a comparison of the SAXS spectrum to previous small angle neutron scattering measurements [35] on similar samples of smaller magnetic size, we deduce the following value for κ_T^0:

$$\kappa_T^0=\frac{\partial}{\partial\Phi}\left[\frac{\Phi}{kT}\frac{\partial\mu(H=0)}{\partial\Phi}\right]\cong 20 \text{ up to } 8\% , \quad (1)$$

where $\mu(H=0)$ is the chemical potential of the solution in zero field, k the Boltzmann constant, and T the temperature.

The reduced parameter of magnetic dipole-dipole interaction

$$\gamma=\mu_0 m_S^2 V\frac{\Phi}{kT}\simeq 4.1 . \quad (2)$$

Using in this expression the magnetic volume fraction and the magnetic volume $V=\frac{4}{3}\pi R_M^3$, μ_0 being the vacuum permeability.

The initial susceptibility of the concentrated sample is measured by the method of Foner and Macniff [36] in order to evaluate *interparticle interactions under field:* $\chi=1.8$.

The experimental optical setup is the same as in Ref. [26]. It is sketched in Fig. 1. The printing grating is built up in the sample with two interfering pump beams produced by a Q-switched, mode-locked, frequency doubled neodymium-doped yttrium aluminum garnet Nd:YAG laser. The device provides 80 μs duration, linearly polarized pulses. They are gathered in groups of about 40 with a 1 kHz repetition rate. The incident mean power is lower than 200 mW. The incident laser beam at 532 nm is split into two beams (L_1,L_1') of equal intensities. They are focused and intersect in the sample (S) cell of 10 μm thickness to produce an interference pattern; its geometric extension is about 3×10^{-7} m^2 with an interfringe Λ which can be varied from 20 to 65 μm. The interference pattern is controlled by an optical projection on a distant screen, the interfringe being adjusted through the angle between the two pump beams. A magnetic field ranging from 0 to 120 kA/m is provided by an electromagnet; it can be applied to the sample parallel to the grating plane, either parallel or perpendicular to the fringes [cf. Figs. 2(a) and 2(b)]. A weaker field (up to 14 kA/m) can also be applied perpendicularly to the grating

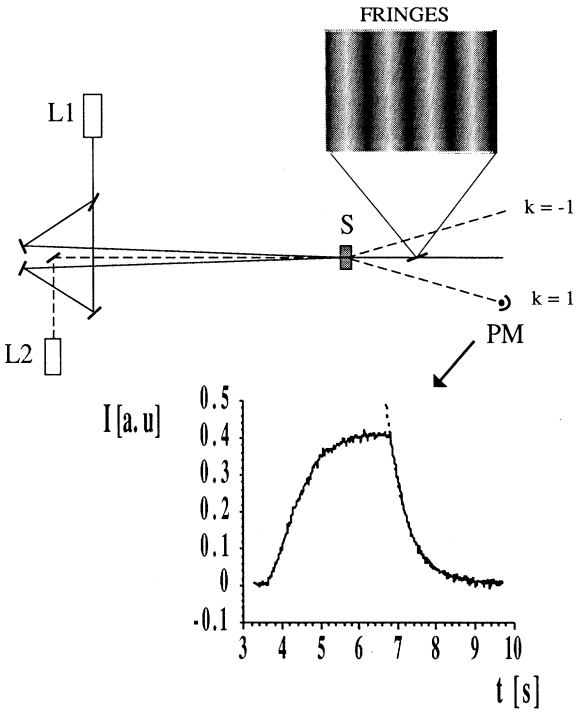

FIG. 1. Optical setup of the forced Rayleigh device.

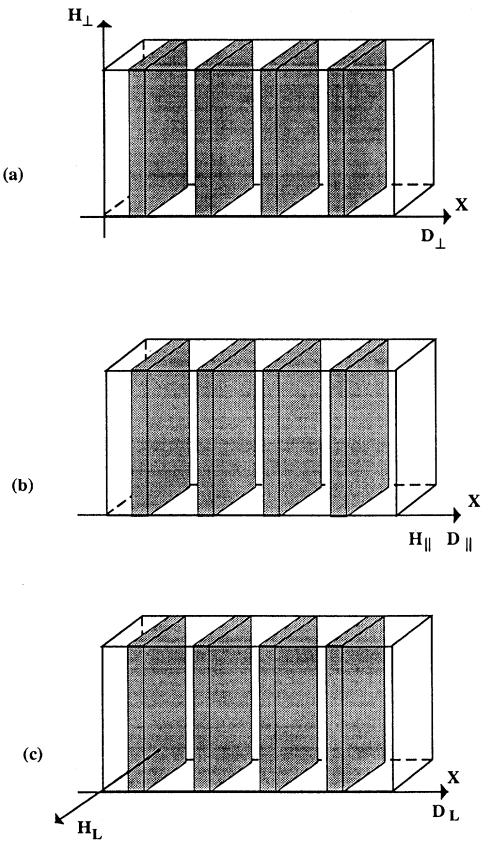

FIG. 2. Scheme of the three geometries of magnetic field. (a) Perpendicular geometry ($\perp$); (b) parallel geometry ($\parallel$); (c) longitudinal geometry (L).

plane, leading to the experimental situation of Fig. 2(c).

A concentration grating can be directly observed in the sample by a red light working microscope [26]. But the precise way to study its evolution is the following. The induced grating is probed (see Fig. 1) by the diffraction of a second laser beam L_2 of lower intensity (He-Ne, 635 nm, 10 mW). The first order diffracted intensity is detected by a photomultiplier tube, the signal being then digitized and computer processed. When the two pump beams are switched on, and whatever the direction and the value of the magnetic field, the diffracted intensity first grows for a few seconds and then saturates (see inset of Fig. 1): this corresponds to the formation of the grating followed by a steady state. When the green pump beams are switched off, the scattered red light intensity decreases exponentially with time, proving the vanishing of the transient grating. The process leading to the grating formation is complex, mixing both thermophoretic and electrophoretic effects [2,37–39]: the interference pattern induces a gradient of electric field and a gradient of temperature. They both lead to a net force on the particles but the light absorption of the particles is essential to the formation of the concentration grating. The details of this process will be studied in a forthcoming paper. In contrast, the relaxation process is simple. The relaxation time τ_D of the signal is always much larger than all the thermal typical times of the system (thermal relaxation nanoparticle-solvent 1 ps; thermal relaxation of a 30 μm grating 1 ms). It is directly related to the translational diffusion coefficient of the particles [26]. The measured scattered intensity [25] can be written as a function of both a background noise (a contribution), mainly due to dust inside the sample, and an exponential decay term (proportional to b) due to the diffusion of particles:

$$I \propto (a + be^{-Dq^2t})^2 , \tag{3}$$

where D is the diffusion coefficient of the particles, $q = 2\pi/\Lambda$ is the experimental wave vector given by the interfringe Λ, and t is time. Experimentally the detection is homodyne ($a \ll b$) and the relaxation of the signal can be analyzed with one relaxation time τ_D, inversely proportional to q^2 [see Fig. 3(a) and Ref. [26]] which proves the total lack of recombination processes [40,41] and allows us to define an experimental diffusion coefficient

$$D^{\text{expt}} = (2\tau_D q^2)^{-1} . \tag{4}$$

It depends on both the strength and geometry of the applied magnetic field. Figure 3 is a plot of τ_D^{-1} versus q^2 for various magnetic field strengths in the perpendicular and parallel geometries [magnetic field direction perpendicular or parallel to the concentration gradient, respectively, and parallel to the fringe plane in both cases, the geometry of Figs. 2(a) and 2(b)]. The values of the diffusion coefficients $D_\perp^{\text{expt}}(H)$ and $D_\parallel^{\text{expt}}(H)$ are given by the slopes of these plots from Eq. (4). Variations of D_L^{expt} as a function of H are determined from similar plots in the geometry of Fig. 2(c).

In zero magnetic field [26], we find $D_0^{\text{expt}} = 2.7 \times 10^{-11}$ m^2 s^{-1}, a value compatible with a hard sphere model with thermodynamic interactions. For a finite volume fraction

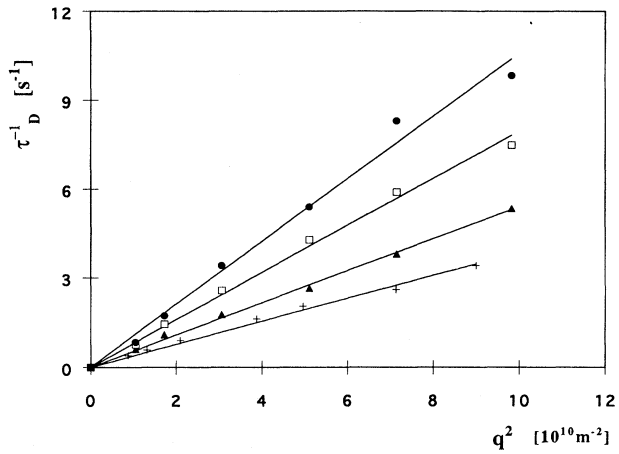

FIG. 3. Plots of τ_D^{-1} as a function of q^2 for various applied fields in geometries ($\parallel$) and ($\perp$) of Fig. 2. $D_\parallel^{\text{expt}}$ (or $D_\perp^{\text{expt}}$) is the slope of the linear best fit. (●) $H_\parallel = 112$ kA/m, $D_\parallel^{\text{expt}} = 5.4 \times 10^{-11}$ m^2 s^{-1}; (□) $H_\parallel = 28$ kA/m, $D_\parallel^{\text{expt}} = 4 \times 10^{-11}$ m^2 s^{-1}; (▲) $H = 0$, $D_0^{\text{expt}} = 2.7 \times 10^{-11}$ m^2 s^{-1}; (+) $H_\perp = 112$ kA/m, $D_\perp^{\text{expt}} = 1.9 \times 10^{-11}$ m^2 s^{-1}.

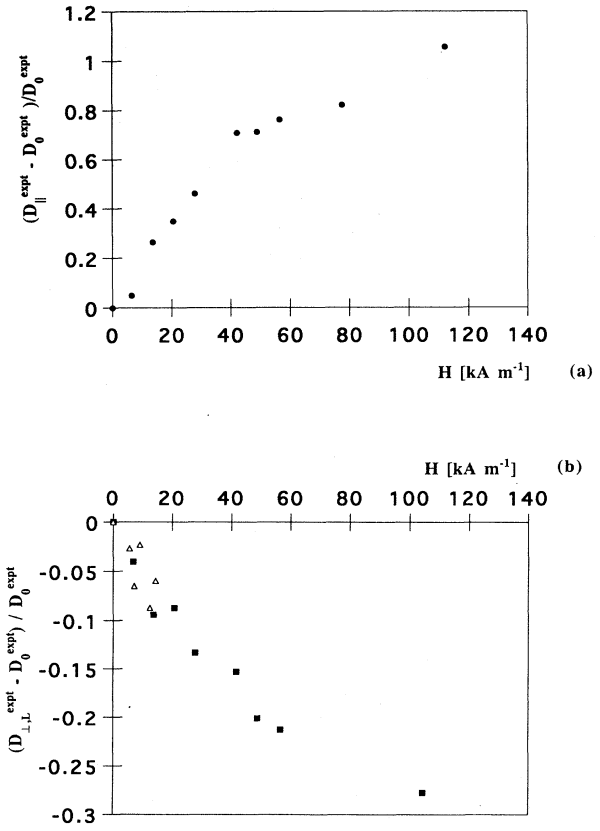

FIG. 4. Reduced variations of D^{expt} as a function of applied magnetic field H. (a) Reduced variation of $D_\parallel^{\text{expt}}$ (black dots); (b) reduced variation of $D_\perp^{\text{expt}}$ (black squares) and of D_L^{expt} (open triangles).

Φ of colloidal particles and in the linear regime, the generalized Stokes formula for the diffusion coefficient is

$$D_0(\Phi)=\frac{\Phi}{f(\Phi)}\frac{\partial}{\partial\Phi}[\mu(H=0)]$$
$$\cong\frac{kT}{6\pi\eta_0 R_H}[1+(\kappa_T-\kappa_f)\Phi]\ , \tag{5}$$

$f(\Phi)=6\pi\eta_0 R_H(1+\kappa_f\Phi)$ being the friction coefficient, η_0 the viscosity of the fluid carrier (here water), and the coefficients κ_T and κ_f accounting respectively for thermodynamic and hydrodynamic interactions; for hard spheres [42], $\kappa_f=6.55$. If we identify D_0^{expt} with $D_0(\Phi)$ (thus assuming a linear description up to $\Phi=10\%$) we obtain $\kappa_T=16$, very close to the former evaluation [cf. Eq. (1)] $\kappa_T^0=20$ from Ref. [35].

Reduced variations of the three different diffusion coefficients $D_\perp^{\text{expt}}(H)$, $D_\parallel^{\text{expt}}(H)$, and D_L^{expt} are plotted as a function of magnetic field strength in Figs. 4(a) and 4(b). If $D_\parallel^{\text{expt}}$ is an increasing function of the applied field, on the contrary both $D_\perp^{\text{expt}}$ and D_L^{expt} are decreasing functions of the field. Within the experimental accuracy of the diffusion coefficient determination, which ranges from 2% for $H=0$ to 5% for $H=120$ kA/m, we do not detect any difference between $D_\perp^{\text{expt}}$ and D_L^{expt} values at equivalent fields. In the next section, we develop a theoretical model accounting for the field dependence of these three diffusion coefficients.

III. THEORETICAL SECTION

Decoupling, because of their largely different time scales, thermal and mass diffusion fluxes, the evolution of particle volume fraction is driven in one dimension by the Fick law

$$\frac{\partial\Phi}{\partial t}=-\frac{\partial j_x}{\partial x}\ , \tag{6}$$

where j_x is the diffusion flow equal to

$$j_x=-\Phi\frac{\partial\mu}{\partial x}\frac{1}{f(\Phi)} \tag{7}$$

with μ the chemical potential of magnetic particles. These two equations (6) and (7) allow a determination of the diffusion coefficient in the presence of a field, the chemical potential being written as a sum of two terms [3,43,44]:

$$\mu=\mu(H=0)+\mu_H\ . \tag{8}$$

A dilute magnetic colloid without interparticle interactions is paramagnetic and its magnetization M is given by the Langevin law

$$M=\Phi m_s L(\xi) \tag{9}$$

with $\xi=\mu_0 m_s VH/kT$ the Langevin parameter and the Langevin function $L(\xi)=\coth(\xi)-\xi^{-1}$. In order to take into account the magnetic interparticle interactions under the applied field, we use, in a mean field approximation, an effective field model, and the expression (9) becomes [2,3,43,44]

$$M=\Phi m_s L(\xi_e) \tag{10}$$

with ξ_e given by the self-consistent equation

$$\xi_e=\xi+\lambda\gamma L(\xi_e)\ , \tag{11}$$

where γ is the reduced parameter of dipolar interaction [cf. Eq. (2)] and λ the effective field constant. If $\lambda=0$, expressions without interparticle interactions under the field are recovered. The classical Lorentz value [45] of λ is 0.33.

To solve Eqs. (6) and (7), it is necessary to calculate $\partial\mu/\partial x$:

$$\frac{\partial\mu}{\partial x}=\underbrace{\frac{\partial\mu(H=0)}{\partial\Phi}\frac{\partial\Phi}{\partial x}}_{\text{(i)}}+\underbrace{\left[\frac{\partial\mu_H}{\partial\Phi}\right]_H\frac{\partial\Phi}{\partial x}}_{\text{(ii)}}+\underbrace{\left[\frac{\partial\mu_H}{\partial H}\right]_\Phi\frac{\partial H}{\partial x}}_{\text{(iii)}}\ . \tag{12}$$

Term (i) is the usual one leading to the generalized Stokes diffusion coefficient in zero field [see Eq. (5)]. Term (ii) is related to magnetic interactions in constant fields and exists whatever the field geometry. The magnetic contribution μ_H to the chemical potential can be written in a mean field approximation [2,3,43,44]

$$\mu_H=-kT\ln(\sinh\xi_e/\xi_e)\ .$$

Thus

$$\left[\frac{\partial\mu_H}{\partial\Phi}\right]_H=-\frac{kT}{\Phi}\alpha_\lambda(\Phi,H) \tag{13}$$

with

$$\alpha_\lambda(\Phi,H)=\frac{\lambda\gamma L^2(\xi_e)}{1-\lambda\gamma L'(\xi_e)}\ ,$$

$L'(\xi_e)$ being the first derivative of the Langevin function $L(\xi_e)$. It must be pointed out that $\alpha_\lambda(\Phi,H)$ is equal to zero for $\lambda=0$, or for $\gamma=0$, or for $H=0$.

Term (iii) basically depends on the magnetic field geometry with respect to the magnetic grating. In the geometries ($\perp$) and (L) of Figs. 2(a) and 2(c), **H** is spatially homogeneous and $\partial H/\partial x=0$. On the contrary in the geometry ($\parallel$) of Fig. 2(b), there are spatial inhomogeneities of H leading to a gradient $\partial H/\partial x$ not equal to zero [26,46].

A. Magnetic field perpendicular to the diffusion direction (geometries $\perp$ and L)

By replacing the three terms (i), (ii), and (iii) in Eq. (7), we obtain

$$j_x^{\perp,L}=-\frac{kT}{f(\Phi)}\frac{\partial\Phi}{\partial x}\left[\frac{\Phi}{kT}\frac{\partial\mu(H=0)}{\partial\Phi}-\alpha_\lambda(\Phi,H)\right]\ . \tag{14}$$

Replacing (14) in Eq. (6) and performing an expansion in the limit of small variations of volume fractions with respect to the equilibrium one Φ, we obtain a diffusion coefficient $D_{\perp,L}$ of particles perpendicular to the magnetic field equal to

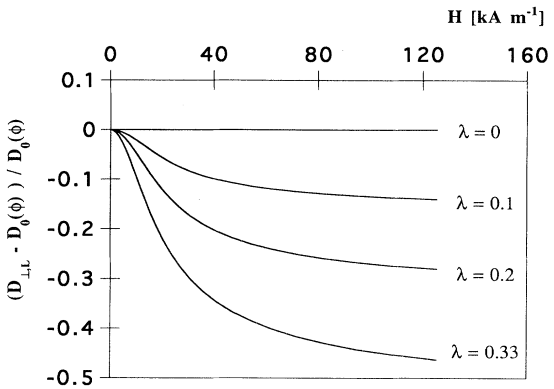

FIG. 5. Reduced variation of $D_\perp$ (or equivalently D_L) as a function of H, deduced from theoretical expression (15) with $\gamma=4.12$, $D_0(\Phi)=D_0^{\text{expt}}=2.7\times10^{11}$ m^{2}s^{-1}, $kT/f(\Phi)=D_0^{\text{expt}}/2.6$ for $\lambda=0$, 0.1, 0.2, and the Lorentz value 0.33.

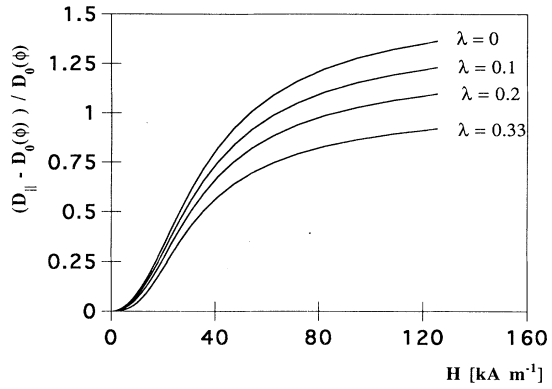

FIG. 6. Reduced variation of $D_\parallel$ as a function of H, deduced from theoretical expression (18) with the same values of the various parameters as in Fig. 5.

$$D_{\perp,L}=D_0(\Phi)-\frac{kT}{f(\Phi)}\alpha_\lambda(\Phi,H)\ . \tag{15}$$

$D_\perp$ and D_L are, as is observed experimentally, decreasing functions of the magnetic field. There are plotted in Fig. 5 for various values of the parameter λ with $\gamma=4.1$ [cf. Eq. (2)], identifying D_0^{expt} with $D_0(\Phi)$ and $D_0(\Phi)/(1+\kappa_T\Phi)$ with $kT/f(\Phi)$, meaning a numerical value of $D_0^{\text{expt}}/2.6$. In reality, due to demagnetizing effects, the term $\alpha_\lambda(\Phi,H)$ is, for the same applied field, slightly smaller for the geometry (L) than for the geometry ($\perp$). We neglect these effects in the present description as the experimental field range of D^L_{expt} is very small in comparison to the one of $D^\perp_{\text{expt}}$.

B. Magnetic field parallel to the diffusion direction (geometry ∥)

In this geometry the term (iii) is not equal to zero. Using the Maxwell relation $(\partial\mu/\partial H)_\phi=-\mu_0 V(\partial M/\partial\Phi)_H$, we have

$$\left[\frac{\partial\mu}{\partial H}\right]_\Phi=-\frac{\mu_0 V m_s L(\xi_e)}{1-\lambda\gamma L'(\xi_e)}\ .$$

From the Maxwell equation in the magnetostatic approximation $\partial(H+M)/\partial x=0$, we can write

$$\frac{\partial H}{\partial x}=-\frac{\partial\Phi}{\partial x}\frac{m_s L(\xi_e)}{1+(1-\lambda)\gamma L'(\xi_e)}\ ,$$

which leads to

$$\left[\frac{\partial\mu_H}{\partial H}\right]_\Phi=\frac{kT}{\Phi}\beta_\lambda(\Phi,H)\frac{\partial\Phi}{\partial x}$$

with

$$\beta_\lambda(\Phi,H)=\frac{\gamma L^2(\xi_e)}{[1-\gamma\lambda L'(\xi_e)][1+(1-\lambda)\gamma L'(\xi_e)]}\ . \tag{16}$$

$\beta_\lambda(\Phi,H)$ is equal to zero either for $\gamma=0$ or for $H=0$ but is equal [26]to $\gamma L^2(\xi_e)/[1+\gamma L'(\xi_e)]$ for $\lambda=0$. Then Eq. (14) transforms to

$$j_x^{\parallel}=-\frac{kT}{f(\Phi)}\frac{\partial\Phi}{\partial x}\left[\frac{\Phi}{kT}\frac{\partial\mu(H=0)}{\partial\Phi}-\alpha_\lambda(\Phi,H)+\beta_\lambda(\Phi,H)\right] \tag{17}$$

and Eq. (15) to

$$D_\parallel=D_0(\Phi)+\frac{kT}{f(\Phi)}[\beta_\lambda(\Phi,H)-\alpha_\lambda(\Phi,H)]\ . \tag{18}$$

Reduced variations of $D_\parallel$ as a function of the strength of the applied magnetic field are plotted in Fig. 6 for various values of the parameter λ with experimental values of $\gamma=4.1$, with $D_0(\Phi)=D_0^{\text{expt}}$ and $kT/f(\Phi)=D_0^{\text{expt}}/2.6$. As is observed experimentally, $D_\parallel$ is an increasing function of H.

IV. DISCUSSION

From the representations of Figs. 5 and 6, it is clear that interparticle interactions under a field, through the mean field parameter, lower the translational diffusion coefficient whatever the field geometry, parallel, perpendicular, or longitudinal. For the three geometries, the experimental results of Figs. 4(a) and 4(b) are between the two theoretical curves for $\lambda=0$ and 0.33. A best fit of these experimental values to both expressions (15) and (18) leads to a value of $\lambda=0.22\pm0.02$. This fit is presented with the two theoretical limits $\lambda=0$ and $\lambda=0.33$ in Fig. 7.

From a comparison of the initial magnetic susceptibility χ of the concentrated sample to the susceptibility χ_0 of a dilute solution of the same sample (volume fraction Φ_0), it is possible to derive another evaluation of magnetic interparticle interactions. In the limit $\xi\ll1$ and $\xi_e\ll1$, Eqs. (9)–(11) lead to

$$\chi=\frac{\gamma}{3(1-\lambda\gamma/3)}\ . \tag{19}$$

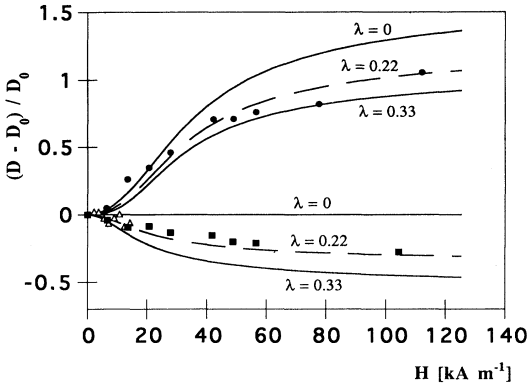

FIG. 7. Reduced variations of the various diffusion coefficients as a function of the magnetic field strength H. Comparison of experiments to the theoretical expressions (15) and (18). Black dots: experiments in the parallel geometry (∥) of Fig. 2(b). Black squares: experiments in the perpendicular geometry (⊥) of Fig. 2(a). Open triangles: experiments in the longitudinal geometry (L) of Fig. 2(c). Full line: expressions (15) and (18) with $\lambda=0$ and experimental values of the other parameters. Dotted line: expressions (15) and (18) with $\lambda=0.33$ and experimental values of the other parameters. Dashed line: best fit of the experiments in the various geometries to theoretical expressions (15) and (18) with $\gamma=4.1$, $D_0(\Phi)=D_0^{\text{expt}}=2.7\times10^{11}$ m^{2}s^{-1}, $kT/f(\Phi)=D_0^{\text{expt}}/2.6$, leading to $\lambda=0.22\pm0.02$.

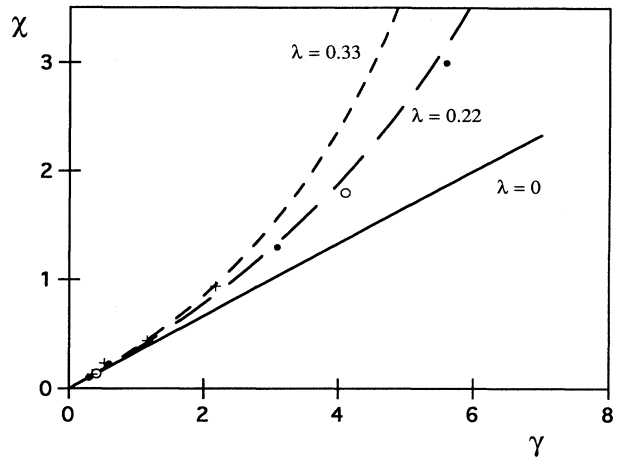

FIG. 8. Initial susceptibility as a function of γ. (○) Ferrofluid sample used in the forced Rayleigh experiment; (+) ferrofluid sample of Ref. [35]; (●) ferrofluid sample of Ref. [47]; (full line) expression (19) with $\lambda=0$; (dashed line) expression (19) with $\lambda=0.22$; (dotted line) expression (19) with $\lambda=0.33$.

From the present forced Rayleigh experiment, we deduce $\chi\simeq1.95$, in rather good agreement with the direct measurement $\chi\simeq1.8$. The representation of Fig. 8 definitely confirms the experimental determination of the λ parameter. The initial susceptibility χ is plotted as a function of γ for various ferrofluid samples (the present one and samples from Refs. [35] and [47]); γ is proportional to the concentration Φ of the solution. The ratio γ/Φ is a constant independent of Φ, deduced, for each particle size, from the low concentration behavior of χ: $\gamma/\Phi=\mu_0 m_s^2 V/kT\simeq3\chi/\Phi$ if $\Phi\to0$ ($\Phi<1\%$). For a comparison, the theoretical expression (19) is also plotted for three values of λ, 0, 0.22, and 0.33. The value $\lambda=0.22$, which is deduced from the best fit of diffusion coefficients under a field, also fits quite well the χ variations, demonstrating the self-consistency of our theoretical description.

V. CONCLUSION

A transient grating experiment is performed with a concentrated ferrofluid solution ($\Phi\simeq10\%$) in the presence of an external magnetic field. Various geometries are explored: in the plane of the transient grating, either parallel or perpendicular to the fringes, and perpendicular to the transient grating.

Whatever the direction and the strength (up to 120 kA/m) of the magnetic field, the relaxation of the first order diffracted intensity of a probing laser beam is diffusive, characteristic of a diffusion process. A mean field model taking into account the magnetic interactions between particles under a field well predicts the field dependence of the three different diffusion coefficients.

We have thus demonstrated here that it is possible with this experiment to measure several parameters of interparticle interaction: the second virial of osmotic pressure κ_T or the effective field constant λ. In the future, this powerful technique will be used to determine the effect on κ_T or λ of some other parameters of the magnetic colloid, such as the ionic strength of the solution, the particle size, or the particle concentration. This knowledge will be of paramount importance from the point of view of technical applications.

ACKNOWLEDGMENTS

We thank V. Cabuil and S. Neveu for providing us with the magnetic fluid sample. One of us (B. Kashevsky) thanks the Ministère de l'Enseignement Supérieur et de la Recherche (M.E.S.R.) of France for financial support. This work was supported by "Le réseau Formation-Recherche" No. 90R0933 of MESR and by the long term Grant No. LBG000 of the International Science Foundation. The Laboratoire d'Acoustique et Optique de la Matière Condensée is associated with the Centre National de la Recherche Scientifique.

[1] R. E. Rosensweig, *Ferrohydrodynamics* (Cambridge University Press, Cambridge, England, 1985).
[2] E. J. Blums, A. O. Cebers, and M. M. Mayorov, *Magnetic Fluids* (Zinatne, Riga, Latvia, 1989) (in Russian).
[3] *Magnetic Fluids and Applications—Handbook,* edited by B. Berkovsky and M. Krakov (Begel-House, New York, 1994).
[4] Proceedings of ICMF 6, Paris, 1992, edited by V. Cabuil, J.-C. Bacri, and R. Perzynski (Elsevier, Amsterdam, 1993).
[5] R. E. Rosensweig, M. Zahn, and R. Shumovich, J. Magn. Magn. Mater. **39**, 127 (1983).
[6] D. P. Jackson, R. E. Goldstein, and A. Cebers, Phys. Rev. E **50**, 298 (1994).
[7] J.-C. Bacri, A. Cebers, and R. Perzynski, Phys. Rev. Lett. **72**, 2705 (1994).
[8] J.-C. Bacri, A. Cebers, J.-C. Dabadie, and R. Perzynski, Europhys. Lett. **27**, 437 (1994); Phys. Rev. E **50**, 2712 (1994).
[9] S. Douady and Y. Couder, Phys. Rev. Lett. **68**, 2098 (1992).
[10] P. Fabre, C. Casagrande, M. Veyssié, V. Cabuil, and R. Massart, Phys. Rev. Lett. **64**, 539 (1990).
[11] J.-C. Bacri and A. M. Figueiredo Neto, Phys. Rev. E **50**, 3860 (1994).
[12] S. V. Burlyov and Yu. L. Raikher, Phys. Rev. E **50**, 358 (1994).
[13] J. Bibette, J. Magn. Magn. Mater. **122**, 37 (1993).
[14] V. Cabuil and C. Ménager, J. Colloid Interface Sci. **169**, 251 (1995).
[15] J.-C. Bacri, V. Cabuil, A. Cebers, C. Ménager, and R. Perzynski, Mater. Sci. Eng. C (to be published).
[16] M. M. Maiorov, Magn. Gidrodin. **3**, 29 (1977).
[17] P. Scholten, IEEE Trans. Magn. **MAG-11**, 1400 (1975); **MAG-16**, 221 (1980).
[18] W. Davies and J. P. Llewellyn, J. Phys. D **13**, 2327 (1980).
[19] J.-C. Bacri, J. Dumas, D. Gorse, R. Perzynski, and D. Salin, J. Phys. (Paris) Lett. **46**, L119 (1985).
[20] J.-C. Bacri, R. Perzynski, D. Salin, and J. Servais, J. Phys. (Paris) **48**, 1385 (1987).
[21] P. Fabre, C. Quilllet, M. Veyssié, F. Nallet, D. Roux, V. Cabuil, and R. Massart, Europhys. Lett. **20**, 229 (1992).
[22] J. Popplewell, in Abstracts of ICMF6 Paris, 1992, p. 344 (Elsevier, Amsterdam, 1993).
[23] V. Cabuil, N. Hochart, R. Perzynski, and P. J. Lutz, Prog. Colloid Polymer. Sci. **97**, 71 (1994).
[24] V. T. Lebedev, G. P. Gordeev, E. A. Panasiuk, L. Kiss, L. Cser, L. Rosta, Gy. Török, and B. Farago, J. Magn. Magn. Mater. **122**, 83 (1993).
[25] H. Hervet, L. Léger, and R. Rondelez, Phys. Rev. Lett. **42**, 1681 (1979).
[26] J.-C. Bacri, A. Cebers, A. Bourdon, G. Demouchy, B. M. Heegaard, and R. Perzynski, Phys. Rev. Lett. **73**, 5032 (1995).
[27] J.-C. Bacri, R. Perzynski, D. Salin, V. Cabuil, and R. Massart, J. Colloid Interface Sci. **132**, 43 (1989).
[28] R. E. Rosensweig and J. Popplewell, in *Electromagnetic Forces and Applications,* Elsevier Studies in Applied Electromagnetic in Materials Vol. 1 (Elsevier, Amsterdam, 1992), p. 83.
[29] For a review, see V. Cabuil, Yu. Raikher, J.-C. Bacri, and R. Perzynski, in *Magnetic Fluids and Applications—Handbook* [3], p. 31.
[30] W. B. Russel, D. A. Saville, and W. R. Schowalter, *Colloidal Dispersions* (Cambridge University Press, Cambridge, England, 1989).
[31] R. Massart, IEEE Trans. Magn. **MAG-17**, 1247 (1981).
[32] J.-C. Bacri, V. Cabuil, P. Lesieur, and R. Perzynski (unpublished).
[33] J.-C. Bacri, R. Perzynski, D. Salin, V. Cabuil, and R. Massart, J. Magn. Magn. Mater. **85**, 27 (1990).
[34] R. W. Chantrell, J. Popplewell, and S. W. Charles, IEEE Trans. Magn. **MAG-14**, 975 (1978).
[35] J.-C. Bacri, F. Boué, V. Cabuil, and R. Perzysnki, Colloids Surf. A **80**, 11 (1993).
[36] S. Foner and E. J. Macniff, Jr., Rev. Sci. Instrum. **39**, 171 (1968).
[37] M. M. Burns, J. M. Fournier, and J. A. Golovchenko, Science **249**, 749 (1990).
[38] J. P. Delville, C. Lalaude, E. Freysz, and A. Ducasse, Phys. Rev. E **49**, 4145 (1994).
[39] E. Blums, Magn. Gidrodin. **1**, 23 (1979).
[40] H. J. Eichler, Opt. Acta **24**, 631 (1977).
[41] A. Bourdon, J. Duran, F. Pellé, and D. de Viry, Phys. Rev. B **30**, 7105 (1984).
[42] G. K. Batchelor, J. Fluid Mech. **119**, 379 (1982).
[43] L. D. Landau and E. M. Lifshitz, *Electrodynamics of Continuous Media* (Pergamon, New York, 1959).
[44] A. O. Cebers, Magn. Gidrodin. **2**, 42 (1992).
[45] C. Kittel, *Introduction to Solid State Physics* (Wiley, New York, 1967), p. 373.
[46] A. Cebers, Magn. Gidrodin. **2**, 3 (1991).
[47] C. H. des Villettes, DEA report, Université Pierre et Marie Curie, France, 1991 (unpublished).

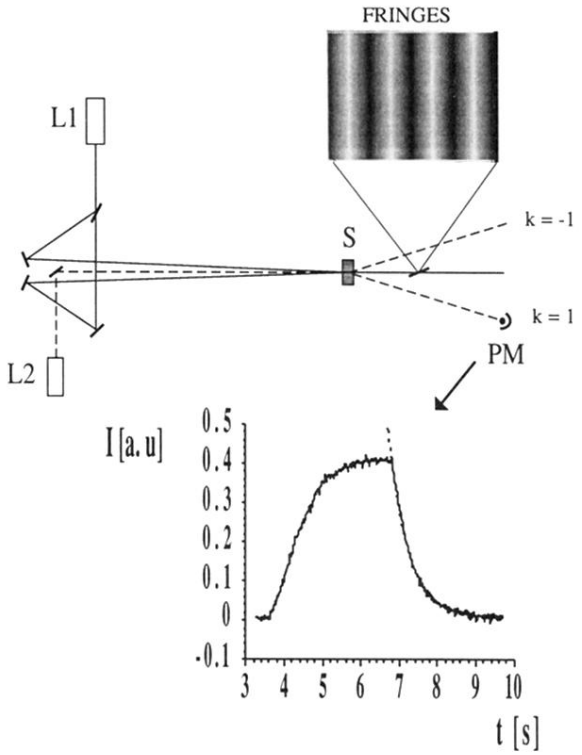

FIG. 1. Optical setup of the forced Rayleigh device.